NANO LETTERS

2008
Vol. 8, No. 3
919-924

Simultaneous Measurements of Electronic Conduction and Raman Response in Molecular Junctions

Daniel R. Ward,[†] Naomi J. Halas,[‡,§,||] Jacob W. Ciszek,[⊥] James M. Tour,[§] Yanpeng Wu,[#] Peter Nordlander,[†,||] and Douglas Natelson*,[†,‡,||]

Department of Physics and Astronomy, Department of Electrical and Computer Engineering, Department of Chemistry, Applied Physics Graduate Program, and Rice Quantum Institute, Rice University, 6100 Main Street, Houston, Texas 77005, and Department of Chemistry, Northwestern University, Evanston, Illinois 60208

Received December 20, 2007

ABSTRACT

Electronic conduction through single molecules is affected by the molecular electronic structure as well as by other information that is extremely difficult to assess, such as bonding geometry and chemical environment. The lack of an independent diagnostic technique has long hampered single-molecule conductance studies. We report simultaneous measurement of the conductance and the Raman spectra of nanoscale junctions used for single-molecule electronic experiments. Blinking and spectral diffusion in the Raman response of both *p*-mercaptoaniline and a fluorinated oligophenylyne ethynylene correlate in time with changes in the electronic conductance. Finite difference time domain calculations confirm that these correlations do not result from the conductance modifying the Raman enhancement. Therefore, these observations strongly imply that multimodal sensing of individual molecules is possible in these mass-producible nanostructures.

The molecular-scale limits of electronic conduction are of fundamental scientific interest and relevant to future technologies. Our understanding of electronic conduction through single small molecules has grown dramatically in the past decade thanks to improved techniques, including mechanical break junctions,[1–3] single-molecule transistors (SMTs),[4–19] nanoparticle dimers,[20] noise characterization,[21] and thermopower measurement.[22] A major complication in interpreting these experiments is the lack of local imaging or spectroscopic tools that can assess the environment and presence of the molecule of interest.

Over the same period, single-molecule spectroscopies have progressed substantially. In particular, surface-enhanced Raman spectroscopy (SERS) has been demonstrated with single-molecule sensitivity[23–26] in random aggregates of metal nanoparticles, though this level of detection is very challenging to prove conclusively. The electromagnetic component of SERS enhancement results from the excitation of surface plasmons in the metal, leading to local fields at the molecule enhanced by a factor of $g(\omega)$ relative to the incident field. The Raman cross section is then enhanced by $g(\omega)^2 g(\omega')^2$, where ω and ω' are the frequencies of the incident and Raman-scattered radiation, respectively. Electromagnetic SERS enhancements exceeding 10^{12} are needed to approach single-molecule detection for many molecules without resonant Raman effects.[27] Additional "chemical" enhancement is also possible due to electronic interactions between the molecule and the metal. The vibrational modes observed in SERS reflect both the molecule and the local environment and conformation of the molecule on the metal surface. With a sharp tip to provide a very large local field enhancement, Raman sensitivity has approached the single-molecule level.[28,29] Very recently we found that nanoscale gaps between extended electrodes are very effective as extremely confined SERS hotspots and may be mass produced with relatively high yields.[30]

In this paper we use these nanoscale gap structures to perform simultaneous measurements of electronic transport and SERS. In many previous papers[4–19] it has been established that conductance in such structures is dominated by roughly a molecular volume. The conductance as a function of time is observed to correlate strongly with the SERS signal in 11% of the junctions measured. Conductance changes correlate with sudden changes in the intensity of sets of Raman modes ("blinking") and with spectral diffusion of mode positions. The data suggest that both SERS and conductance changes are most likely due to changes in conformation and binding of an individual molecule. The combined data provide a great deal of information about the effect of molecular orientation and environment on both

---

[*] Corresponding author. E-mail: natelson@rice.edu.
[†] Department of Physics and Astronomy, Rice University.
[‡] Department of Electrical and Computer Engineering, Rice University.
[§] Department of Chemistry, Rice University.
[||] Rice Quantum Institute, Rice University.
[⊥] Department of Chemistry, Northwestern University.
[#] Applied Physics Graduate Program, Rice University.

10.1021/nl073346h CCC: \$40.75

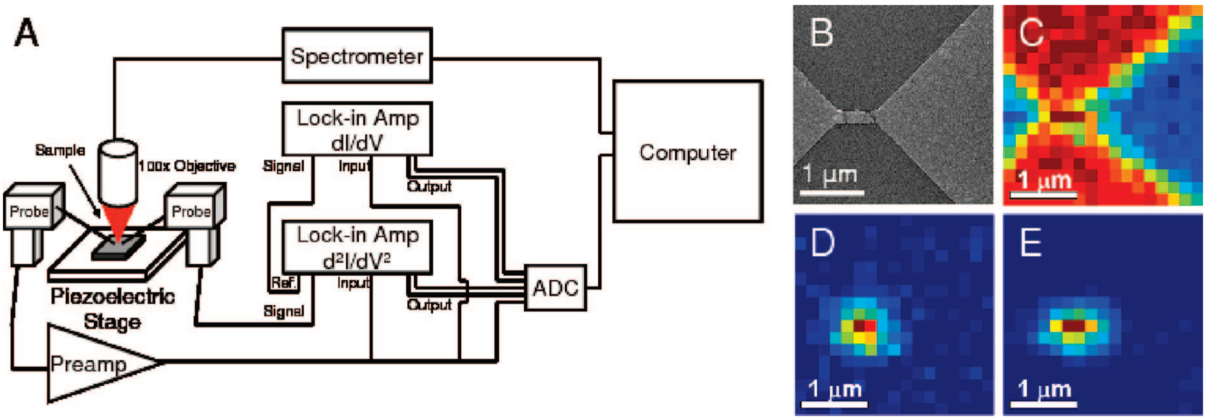

Figure 1. (A) Schematic of the electronic measurement. A 100 mV root mean square ac signal is sourced by a lock-in into one pad. The ac current and its second harmonic are measured by lock-in amplifiers. The dc current is sampled with a current-to-voltage amplifier at 5 kHz. Raman spectra are synchronously captured with 1–2 s integrations at an incident 785 nm wavelength laser intensity of about 0.5 mW. (B) Scanning electron image of Au constriction with nanogap. The constriction is 180 nm wide with a gap <5 nm in size. (C) Map of the substrate Si 520 cm^{-1} peak (integrated from 480 to 560 cm^{-1}) of the device from B. Red corresponds to the highest number of CCD counts and blue represents the fewest counts. The Au pads which attenuate the Si signal are clearly visible. (D) Map of the pMA SERS signal from device in B from the a$_1$ symmetry mode at 1590 cm^{-1} (integrated from 1550 to 1650 cm^{-1}), showing that the Raman signal is localized only to the nanogap region. (E) Map of integrated continuum signal (due to inelastic light scattering from the metal electrodes) from device in B (integrated from 50 to 300 cm^{-1}).

conduction and SERS, although a detailed understanding of this correlated information is indeed a very significant theoretical challenge. The most likely explanation for these results is that single-molecule multimodal sensing is possible. This combined measurement technique also opens the possibility of direct assessment of vibrational pumping and local heating in single-molecule electronic transport.

Our nanogap structures are fabricated on ~1 cm^2 pieces of n+-doped Si wafer with 200 nm of thermal silicon oxide. The structures are defined using electron-beam lithography and e-beam evaporation of 1 nm of Ti and 15 nm of Au. The initial nanoconstriction structure consists of two large pads connected by a single constriction as shown in Figure 1. The constriction is approximately 500 nm long and 100–180 nm wide. Liftoff is performed in acetone or chloroform, and the samples are then cleaned of organic residue by 1 min exposure to O$_2$ plasma. For devices incorporating *p*-mercaptoaniline (pMA), samples are immediately placed in a 1 mM solution of pMA in ethanol. Samples are soaked in the pMA solution for 12−24 h as pMA self-assembles on the Au surfaces, followed by an ethanol rinse to remove any excess pMA. We have also measured devices using a fluorinated oligophenylene ethynylene (FOPE)[31] that possesses a distinctive Raman spectrum (see Supporting Information). FOPE was assembled via standard base deprotection[32] from a 0.25 mg/mL solution of the thioacetate form of the molecules in 1:1 ethanol/chloroform solvent, prepared under dry N$_2$ gas.

The nanoconstrictions are converted into nanogaps via electromigration,[33] a thoroughly studied[34,35] process dominated by momentum transfer from current-carrying electrons to mobile atoms in the metallic lattice. Electromigration has been used extensively to prepare electrodes for single-molecule conduction measurements, with typical yields of ~10–20% for tunneling gaps inferred to contain individual molecules (based on statistics on thousands of junctions).[4–6,8–15,17,18] Each gap is electromigrated with an automated procedure to form an atomic-scale constriction with a resistance of ~3 kΩ, which is then allowed to break spontaneously.[36] While the atomic-scale details of each gap are different, gaps with measurable tunneling currents are formed routinely with high yield, and recent advances in in situ electron microscopy[34,37] do, in principle, permit detailed structural examinations of the resulting electrodes. The migration and subsequent electrical measurements are performed in situ on the sample stage of the Raman measurement system, in air at room temperature.

Electrical contact to the junction under test is made via micropositionable probes. One digital lock-in amplifier (SRS SR830) is used to source 50–100 mV root mean square (rms) at 200 Hz onto one pad, while the other pad is connected to a current-to-voltage converter (either SRS SR570 or Keithley 482). The ac current ($\propto dI/dV$) and its second harmonic ($\propto d^2I/dV^2$) are measured with lock-in amplifiers, while the dc component of the current is sampled at 5.0 kHz. The unusually large ac bias (much larger than necessary to measure differential conductance alone) is required because of an unanticipated complication: the illuminated, molecule-decorated nanogaps can also exhibit significant dc photocurrents due to optical rectification (to be described in a separate publication). The large ac bias is needed so that the ac current is detectable without the dc current signal overloading the lock-in input stages. We find no evidence that the 100 mV rms ac bias degrades the nanogap or the assembled molecules.

Optical measurements are performed using a WITec CRM 200 scanning confocal Raman microscope in reflection mode. Devices are illuminated by a 785 nm diode laser at normal incidence with a diffraction-limited spot. A 100× ultralong working distance objective leaves sufficient room for the micromanipulated electrical probes to be inserted between the objective and sample.

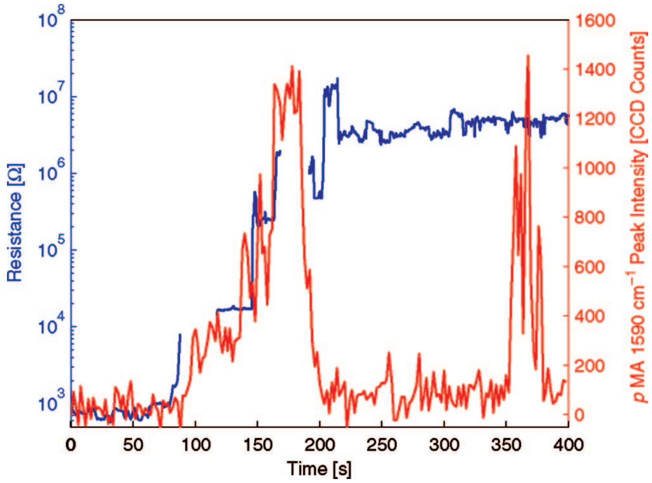

Figure 2. Blue curve (left scale): Resistance as a function of time for a nanogap as it is migrated. Migration is complete when the resistance reaches ~13 kΩ ≈ $(1/G_0)$. Breaks in the curve occur where the gain of the current amplifier was being changed to maintain signal. Red curve (right scale): CCD counts per second in the 1590 cm^{-1} peak (integrated from 1550 to 1650 cm^{-1}) as a function of time for the same device (synchronized with resistance plot). The intensity of the peak increases linearly with the log of the resistance until the resistance reaches around 10^6 Ω, at which point the intensity drops significantly and no shows correlations with the resistance. Stochastic intensity fluctuations ("blinking") are observed beyond this point.

As reported previously, the electromigrated nanogaps are outstanding substrates for SERS.[30] Initially, spatial maps of the underlying Si of unmigrated nanogaps are obtained to facilitate centering of the Raman microscope over the nanogap to within 100 nm. Spatial maps of the integrated molecular Raman signal after electromigration demonstrate the localization of the SERS hotspot (Figure 1D,E). Raman spectra are taken with 1 or 2 s integration times while the microscope objective is held fixed over the migrated junctions. Electrical measurements on unbroken constrictions under various illumination conditions demonstrate that heating of the electrodes due to the laser is not significant. The inferred change in the electrode temperature at ~0.5 mW laser power was less than 2 K (see Supporting Information).

When the conductance of the junction drops below the conductance quantum, $G_0 \equiv 2e^2/h$, a tunneling gap is formed, and simultaneous conductance and Raman measurements are performed. In situ measurements of the optical response of nanogaps during migration are presented in Figure 2. Even prior to complete nanogap formation, partially electromigrated junctions show SERS enhancement of the assembled molecules once the resistance exceeds about 1 kΩ. The appearance of SERS indicates that the local interelectrode plasmon modes are now excitable. Crudely, this implies that over an optical cycle the junction acts more like a capacitor than a resistor; that is, the *RC* time constant of the nanogap is comparable to one optical period. For a 1 kΩ nanogap illuminated at 785 nm, this implies an effective nanogap capacitance at optical frequencies on the order of tens of attofarads.

The measured Raman signal strength scales logarithmically with the resistance of the gap until resistances exceed 1–10 MΩ. At higher gap resistances, the Raman signal takes on a roughly constant value with sporadic changes (corresponding to SERS blinking events). This decoupling of electronic transport and SERS at low conductances is not surprising a priori, since tunneling conductances vary exponentially with gap size, while local plasmonic structure is less sensitive. Blinking events are often not correlated with further changes in junction resistance. This means that molecules are present in a region of strong Raman enhancement, while the molecular-scale tunneling volume dominating interelectrode conductance does not contain molecules that are detectably contributing to the Raman signal. We discuss this further below.

However, in 17 of 120 junctions using pMA and 4 out of 70 junctions using FOPE, there are strong temporal correlations between the fluctuations in the nanogap conductance and changes in the SERS spectrum. This yield is quantitatively consistent with the yield of tunneling gaps containing single molecules inferred in single-molecule transistor measurements. Examples are shown in Figures 3 and 4 (with additional examples in the Supporting Information). In Figure 3A a simple positive correlation between Raman intensity and dI/dV is observed for all Raman modes. In Figure 3B another positive correlation between Raman intensity and differential conductance is observed in a different junction. In this case spectral diffusion of the Raman lines occurs but does not correlate significantly with the conduction. In both parts A and B of Figure 3, the amplitudes (count rates) of strong Raman modes have similar relative changes as the differential conductance.

Figure 4 is an example of a more complicated relationship between the conductance and the SERS spectrum. While sudden changes in the Raman spectrum are correlated in time with changes in the measured conductance, some increases in Raman intensity correlate with increased conductance, while others correlate with decreases in conductance. Additionally, changes in the mode structure of the Raman spectrum clearly correlate with changes in conductance. In region A the Raman spectrum and conductance are constant; when the Raman spectrum changes in region B, a 3-fold increase in conductance is observed, though overall Raman intensity changes only for certain modes. In region C the spectrum changes yet again, and while a weaker Raman spectrum remains, the conduction drops significantly. In region D the same mode structure seen in B returns and the conduction is similar to that seen in B as well. Regions D and E have positive correlations between Raman intensity and conduction with the lowest conduction observed between D and E where the Raman intensity is also lowest. At F a switch from positive to negative correlation between the Raman intensity and conduction occurs and carries over to regions G and H. At region I a small change in the mode structure is observed correlating with a switch to positive intensity conduction correlations, continuing through regions J and K. In region L there is a final change in mode structure resulting in negative intensity conduction correlations exemplified in the three conduction spikes that occur when the Raman spectrum disappears.

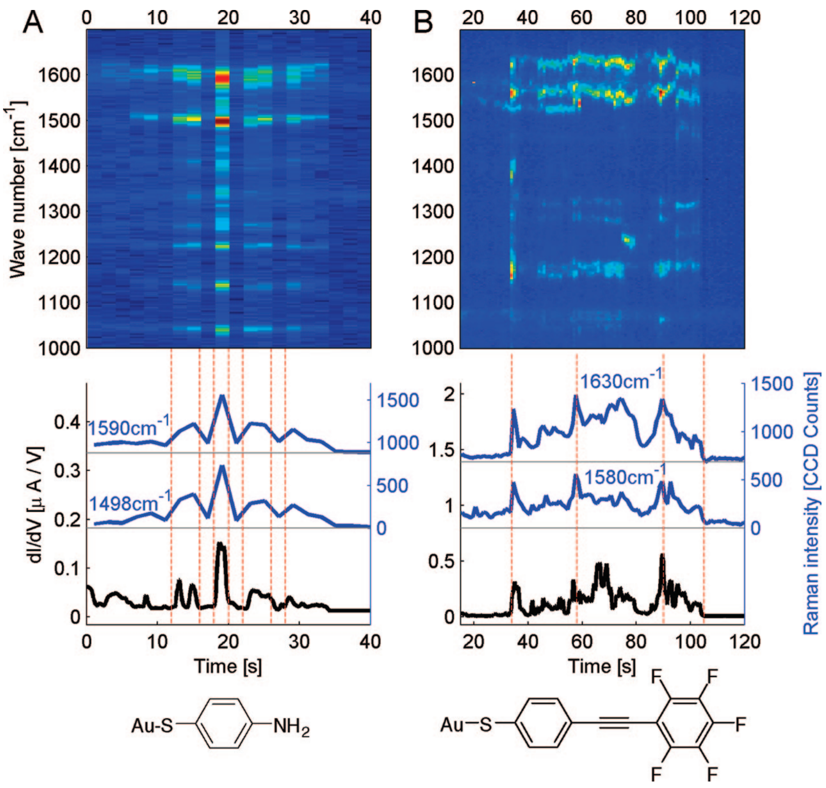

Figure 3. (A) Waterfall plot of Raman spectrum (2 s integrations) and positively correlated differential conductance measurements (dark blue = 50 counts; dark red = 160 counts) for a pMA sample. All Raman modes that are visible exhibit this behavior as illustrated by the 1498 and 1590 cm^{-1} modes. The 1590 cm^{-1} mode has been shifted upward on the lower graph with the gray line indicating zero CCD counts. Vertical red lines indicate points of rapidly changing Raman intensity and conduction. Structure of pMA after self-assembly onto Au is shown below. (B) Waterfall plot of Raman spectrum (1 s integrations) and positively correlated conductance measurement for a FOPE sample (dark blue = 0 counts; dark red = 250 counts). Strong spectral wondering is observed with no correlation to changes in conductance. Both visible modes at 1580 and 1630 cm^{-1} are positively correlated. The slower response of the Raman spectrum compared to the conductance is due to the relatively long integration time. The 1630 cm^{-1} mode has been shifted upward on the lower graph for clarity. Structure of FOPE after self-assembly onto Au is shown below.

It should be noted that our pMA spectra are typically dominated by the b_2 symmetry modes,[38] as was seen previously.[30] This is not surprising, as it is well accepted that b_2 symmetry modes experience additional "chemical" enhancements in comparison to a_1 symmetry modes. We often only observe the 1590 cm^{-1} a_1 symmetry peak and not the other expected a_1 mode at 1077 cm^{-1}. Strong spectral diffusion in both molecules with shifts as large as ±20 cm^{-1} have also been observed, and are clear in Figure 3b. This surely limits direct comparison to spectra reported elsewhere. However, the measured spectra are quite consistent with one another and are qualitatively different than those seen in "bare" junctions contaminated by physisorbed exogenous carbon.[30]

One possible concern could be that changes in metal configuration at the junction are responsible for the fluctuations in tunneling conductance and SERS intensity. This scenario is unlikely for several reasons. First, tunneling conductances depend exponentially on gap geometry; while dI/dV could change by a factor of 10 for a 0.1 nm change in gap separation, it is very unlikely that the electromagnetic enhancement would be as strongly affected. Second, it is not clear how metal rearrangement could explain the observed changes in Figure 4; this would require that the gap itself alternately grow and shrink, with some changes in metal geometry giving large dI/dV features with small Raman effects and others vice versa. Finally, during the events in Figures 3 and 4, the continuum emission at low wavenumbers observed previously due to inelastic light scattering from the metal electrodes[30] is constant in time (see Supporting Information).

Another concern is that changes in tunneling conduction in one part of the junction may alter the plasmon mode structure and affect Raman emission from elsewhere in the junction. Such a scenario could lead to correlations such as those in Figures 3 and 4 even if conduction and Raman emission are not from the same molecule. Given that the interelectrode conductance affects Raman emission (Figure 2), it is important to consider this possibility. We have performed finite difference time domain (FDTD) simulations of the optical properties of such junctions to assess this issue, and the results (vide infra) effectively rule out this concern. While the finite grid size (1 nm) required for practical computation times restricts the quantitative accuracy of these calculations, the main results regarding spatial mode structure and wavelength dependence are robust, and the calculated electric field enhancements are an underestimate.[30,39]

Figure 5 shows a comparison of calculated extinction spectra that characterize the plasmonic mode structure of the gap structure shown, for various values of interelectrode conductance connecting the source and drain at the indicated

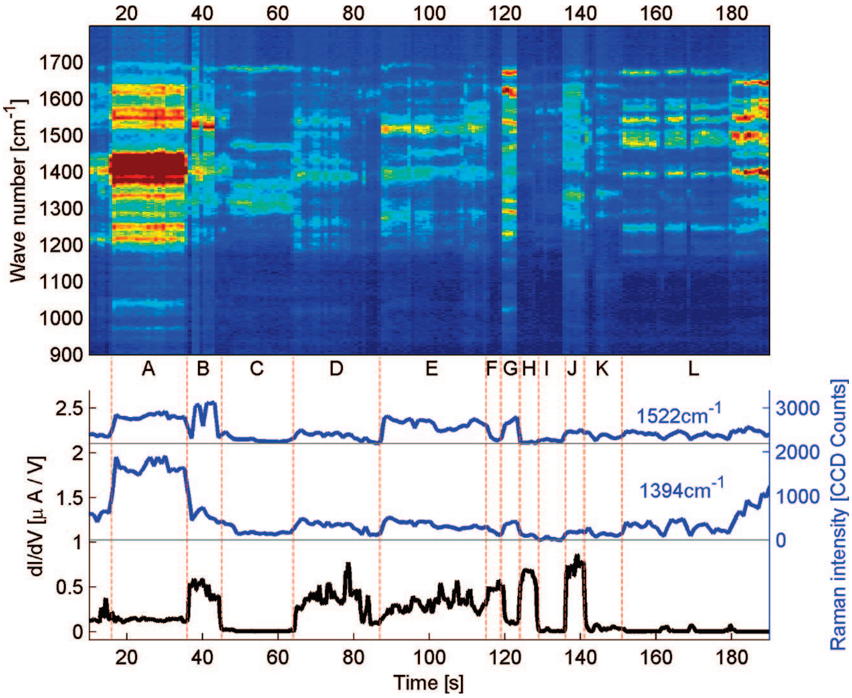

Figure 4. Waterfall plot of Raman spectrum (1 s integrations) and conduction measurements for a pMA sample. The device experiences periods of correlation (regions B, D, E) and anticorrelation (region L) between Raman intensity and conduction. Distinct changes in conduction are observed with every significant change in the Raman spectrum and are indicated by vertical red lines. The modes near 1394 and 1522 cm^{-1} show similar intensity fluctuations except at region B and the end of region L. The color scale (dark blue = 20 counts; dark red = 200 counts) has been set to make as many Raman modes visible as possible. This results in the saturation of the signal at region A which would otherwise resolve into well-defined peaks. The 1522 cm^{-1} mode has been shifted upward on the lower graph for clarity.

point. An analysis of the instantaneous charge distribution associated with the plasmon resonances in Figure 5 shows that negligible charge transfer occurs between the two electrodes for conductances smaller than G_0. The FDTD simulations show that the mode structure and enhancement are unaffected by conductances smaller than a few G_0. Details are presented in Supporting Information. These calculations confirm the interpretation given above for Figure 2: The plasmonic mode structure responsible for enhanced local fields in the nanogap is established once the interelectrode conductance falls well below G_0. Given these FDTD results, the only plausible explanation for such strong correlations in time between conduction and Raman emission is that both processes involve the same molecule or molecules.

Conduction in nanogaps is known to be dominated by a tiny volume inferred in single molecule transport and break junction experiments to contain often only one molecule. Molecular movement, changes in bonding, or reorientation of the molecule in the gap results in different tunneling configurations and hence in conductance changes. The complex relationship between conductance and Raman mode structure and intensity is also then natural, since chemical enhancement effects and the appearance of broken symmetry b_2 modes should be strongly affected by changes in molecular configuration on the metal surface. It should also be noted that the measured junction conductances are consistent with the expected single molecular conductance range of 10^{-1} to 10^{-4} G_0 measured in similar molecules by break junction techniques.[3]

The detailed SERS mode structure combined with the conductance contains a wealth of information about the bonding, orientation, and local environment of the molecule. With appropriate electronic structure calculations and theoretical estimates of the Raman tensor for candidate molecule/metal configurations, it should be possible to infer likely junction geometries and chemical structure corresponding to each type of Raman spectrum. Such calculations are very challenging even for the conductance distribution alone.[40]

These conductance/Raman observations and accompanying calculations demonstrate that electromigrated nanogaps between extended electrodes can achieve enhancements sufficient for single-molecule SERS sensitivity. Given that these structures can be fabricated in a scalable manner in predefined locations with high yields,[30] this may allow significant advances in SERS-based sensing as well as multimodal sensing. With further improvements in technique (e.g., measurements in vacuum as a function of temperature, interelectrode bias, and gate voltage in a SMT configuration), it will be possible to address open fundamental issues in SERS, including the nature of chemical enhancement, the mechanism of blinking, and the cause of the large spectral diffusion of Raman lines. Finally, comparisons of Stokes and anti-Stokes Raman peak intensities as a function of bias across the junction can reveal whether current flow pumps particular vibrational modes out of thermal equilibrium. This would enable new and detailed studies of nonequilibrium physics and chemistry at the single molecule scale. Comparisons between these results and transport/Raman studies on molecular ensembles[41,42] should also provide valuable information about the effect of molecular environment on these processes.

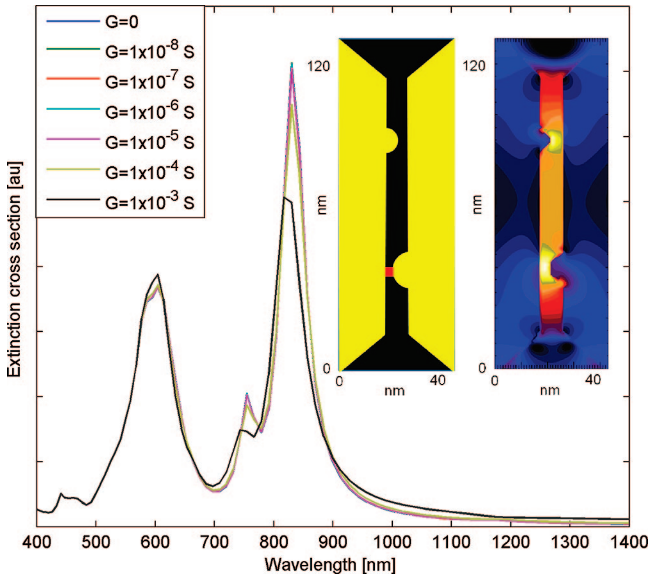

Figure 5. Extinction spectrum calculated using a 1 nm grid size for the structure partially shown in the left inset. The electrodes are modeled as Au, 15 nm thick, sitting on 50 nm thick SiO_2 dielectric, with an overall interelectrode gap of 8 nm. The upper and lower protrusions into that gap shown are modeled as hemispheres of radii 4 and 6 nm, respectively. The red square indicates the location of the modeled interelectrode conductance (a volume 2 nm on a side, meant to represent a molecule at the interelectrode gap). The right inset shows a map of $|E|^4$, where E is the local electric field normalized by the magnitude of the incident field (roughly the Raman enhancement factor), for the mode near 825 nm. White corresponds to an enhancement of 10^9. This field map is essentially unchanged until the junction conductance approachs 10^{-4} S $\sim G_0$.

Acknowledgment. D.W. acknowledges support from the NSF-funded Integrative Graduate Research and Educational Training (IGERT) program in Nanophotonics. N.H., D.N., and P.N. acknowledge support from Robert A. Welch Foundation Grants C-1220, C-1636, and C-1222, respectively. D.N. also acknowledges NSF award DMR-0347253, the David and Lucille Packard Foundation, the Sloan Foundation, and the Research Corporation. J.M.T. acknowledges support from DARPA and AFOSR.

Supporting Information Available: Detailed examination of laser heating, continuum background, extended discussion of FDTD calculations, and more example data sets. This material is available free of charge via the Internet at http://pubs.acs.org.

References

(1) Reed, M. A.; Zhou, C.; Muller, C. J.; Burgin, T. P.; Tour, J. M. *Science* **1997**, *278*, 252–254.
(2) He, J.; Sankey, O.; Lee, M.; Tao, N. J.; Li, X.; Lindsay, S. *Faraday Discuss.* **2006**, *131*, 145–154.
(3) Venkataraman, L.; Klare, J. E.; Tam, I. W.; Nuckolls, C.; Hybertsen, M. S.; Steigerwald, M. L. *Nano Lett.* **2006**, *6*, 458–462.
(4) Park, H.; Park, J.; Lim, A. K. L.; Anderson, E. H.; Alivisatos, A. P.; McEuen, P. L. *Nature* **2000**, *407*, 57–60.
(5) Park, J.; Pasupathy, A. N.; Goldsmith, J. I.; Chang, C.; Yaish, Y.; Petta, J. R.; Rinkowski, M.; Sethna, J. P.; Abruna, H. D.; McEuen, P. L.; Ralph, D. C. *Nature* **2002**, *417*, 722–725.
(6) Liang, W.; Shores, M. P.; Bockrath, M.; Long, J. R.; Park, H. *Nature* **2002**, *417*, 725–729.
(7) Kubatkin, S.; Danilov, A.; Hjort, M.; Cornil, J.; Brèdas, J.-L.; Stuhr-Hansen, N.; Hedegård, P.; Bjørnholm, T. *Nature* **2003**, *425*, 698–701.
(8) Yu, L. H.; Natelson, D. *Nano Lett.* **2004**, *4*, 79–83.
(9) Pasupathy, A. N.; Bialczak, R. C.; Martinek, J.; Grose, J. E.; Donev, L. A. K.; McEuen, P. L.; Ralph, D. C. *Science* **2004**, *306*, 86–89.
(10) Yu, L. H.; K, K. Z.; Ciszek, J. W.; L., C.; Stewart, M. P.; Tour, J. M.; Natelson, D. *Phys. Rev. Lett.* **2004**, *82*, 266802.
(11) Pasupathy, A. N.; Park, J.; Chang, C.; Soldatov, A. V.; Lebedkin, S.; Bialczak, R. C.; Grose, J. E.; Donev, L. A. K.; Sethna, J. P.; Ralph, D. C.; McEuen, P. L. *Nano Lett.* **2005**, *5*, 203–207.
(12) Champagne, A. R.; Pasupathy, A. N.; Ralph, D. C. *Nano Lett.* **2005**, *5*, 305–308.
(13) Yu, L. H.; Keane, Z. K.; Ciszek, J. W.; Cheng, L.; Tour, J. M.; Baruah, T.; Pederson, M. R.; Natelson, D. *Phys. Rev. Lett.* **2005**, *95*, 256803.
(14) Heersche, H. B.; Groot, de Z.; Folk, J. A.; Zant van der, H. S. J.; Romeike, C.; Wegewijs, M. R.; Zobbi, L.; Barreca, D.; Tondello, E.; Cornia, A. *Phys. Rev. Lett.* **2006**, *96*, 206801.
(15) Chae, D.-H.; Berry, J. F.; Jung, S.; Cotton, F. A.; Murillo, C. A.; Yao, Z. *Nano Lett.* **2006**, *6*, 165–168.
(16) Danilov, A. V.; Kubatkin, S. E.; Kafanov, S. G.; Flensberg, K.; Bjørnholm, T. *Nano Lett.* **2006**, *6*, 2184–2190.
(17) Zant, van der, H. S. J.; Osorio, E. A.; Poot, M.; O’Neill, K. *Phys. Status Solidi B* **2006**, *243*, 3408–3412.
(18) Natelson, D.; Yu, L. H.; Ciszek, J. W.; Keane, Z. K.; Tour, J. M. *Chem. Phys.* **2006**, *324*, 267–275.
(19) Danilov, A. V.; Kubatkin, S. E.; Kafanov, S. G.; Hedegård, P.; Stuhr-Hansen, N.; Moth-Poulsen, K.; Bjornholm, T. *Nano Lett.* **2007**, *8*, 1–5.
(20) Dadosh, T.; Gordin, Y.; Krahne, R.; Khivrich, I.; Mahalu, D.; Frydman, V.; Sperling, J.; Yacoby, A.; Bar-Joseph, I. *Nature* **2005**, *436*, 677–680.
(21) Djukic, D.; Ruitenbeek; van, J. M. *Nano Lett.* **2006**, *6*, 789–793.
(22) Reddy, P.; Jang, S.-Y.; Segalman, R. A.; Majumdar, A. *Science* **2007**, *315*, 1568–1571.
(23) Kneipp, K.; Wang, Y.; Kneipp, H.; Perelman, L. T.; Itzkan, I.; Dasari, R.; Feld, M. S. *Phys. Rev. Lett.* **1997**, *78*, 1667–1670.
(24) Nie, S.; Emory, S. R. *Science* **1997**, *275*, 1102–1106.
(25) Xu, H.; Bjerneld, E. J.; Käll, M.; Börjesson, L. *Phys. Rev. Lett.* **1999**, *83*, 4357–4360.
(26) Michaels, A. M.; Jiang, J.; Brus, L. J. *Phys. Chem. B* **2000**, *104*, 11965–11971.
(27) Le Ru, E. C.; Blackie, E.; Meyer, M.; Etchegoin, P. G. J. *Phys. Chem. C* **2007**, *111*, 13794–13803.
(28) Neascu, C. C.; Dreyer, J.; Behr, N.; Raschke, M. B. *Phys. Rev. B* **2006**, *73*, 193406.
(29) Domke, K. F.; Zhang, D.; Pettinger, B. *J. Am. Chem. Soc.* **2006**, *128*, 14721–14727.
(30) Ward, D. R.; Grady, N. K.; Levin, C. S.; Halas, N. J.; Wu, Y.; Nordlander, P.; Natelson, D. *Nano Lett.* **2007**, *7*, 1396–1400.
(31) Hamadani, B. H.; Corley, D. A.; Ciszek, J. W.; Tour, J. M.; Natelson, D. *Nano Lett.* **2006**, *6*, 1303–1306.
(32) Tour, J. M.; Jones, L., II; Pearson, D. L.; Lamba, J. S.; Burgin, T. P.; Whitesides, G. W.; Allara, D. L.; Parikh, A. N.; Atre, S. *J. Am. Chem. Soc.* **1995**, *117*, 9529–9534.
(33) Park, H.; Lim, A. K. L.; Alivisatos, A. P.; Park, J.; McEuen, P. L. *Appl. Phys. Lett.* **1999**, *75*, 301–303.
(34) Strachan, D. R.; Smith, D. E.; Fischbein, M. D.; Johnston, D. E.; Guiton, B. S.; Drndi’c, M.; Bonnell, D. A., Jr *Nano Lett.* **2006**, *6*, 441–444.
(35) Taychatanapat, T.; Bolotin, K.; Kuemmeth, F.; Ralph, D. C. *Nano Lett.* **2007**, *7*, 652–656.
(36) O’Neill, K.; Osorio, E. A.; van der Zant, H. S. J. *Appl. Phys. Lett.* **2007**, *90*, 133109.
(37) Heersche, H. B.; Lientschnig, G.; O’Neill, K.; van der Zant, H. S. J.; Zandbergen, H. W. *Appl. Phys. Lett.* **2007**, *91*, 072107.
(38) Osawa, M.; Matsuda, N.; Yoshii, K.; Uchida, I. *J. Phys. Chem.* **1994**, *98*, 12702–12707.
(39) Oubre, C.; Nordlander, P. *J. Phys. Chem. B* **2005**, *109*, 10042–10051.
(40) Quek, S. Y.; Venkataraman, L.; Choi, H. J.; Louie, S. G.; Hybertsen, M. S.; Neaton, J. B. *Nano Lett.* **2007**, *7*, 3477–3482.
(41) Nowak, A. M.; McCreery, R. L. *J. Am. Chem. Soc.* **2004**, *126*, 16621–16631.
(42) Jaiswal, A.; Tavakoli, K. G.; Zou, S. *Anal. Chem.* **2006**, *78*, 120–124.

NL073346H